Evaluation of wear resistance of a novel carbide-free bainitic steel

Mattia Franceschi, Chiara Soffritti, Annalisa Fortini, Luca Pezzato, Gian Luca Garagnani, Manuele Dabalà

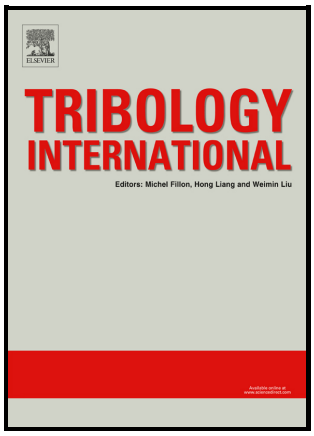

PII: S0301-679X(22)00642-9

DOI: https://doi.org/10.1016/j.triboint.2022.108071

Reference: JTRI108071

To appear in: *Tribology International*

Received date: 26 September 2022
Revised date: 4 November 2022
Accepted date: 13 November 2022

Please cite this article as: Mattia Franceschi, Chiara Soffritti, Annalisa Fortini, Luca Pezzato, Gian Luca Garagnani and Manuele Dabalà, Evaluation of wear resistance of a novel carbide-free bainitic steel, *Tribology International,* (2022) doi:https://doi.org/10.1016/j.triboint.2022.108071

Evaluation of wear resistance of a novel carbide-free bainitic steel

Mattia Franceschi[1,*], Chiara Soffritti[2], Annalisa Fortini[2], Luca Pezzato[1], Gian Luca Garagnani[2], Manuele Dabalà[1]

[1.] Department of Industrial Engineering, University of Padova, Via Marzolo 9, 35131 Padova, Italy; mattia.franceschi@phd.unipd.it (M.F.); luca.pezzato@unipd.it (L.P.); manuele.dabala@unipd.it (M.D.)

[2] Department of Engineering, University of Ferrara, via Saragat 1, 44122, Ferrara, Italy; annalisa.fortini@unife.it (A.F.); chiara.soffritti@unife.it (C.S.); gian.luca.garagnani@unife.it (G.G.)

Abstract

The effect of isothermal transformation temperatures on wear performances of a newly designed high-silicon carbide-free bainitic steel was studied. Wear tests were performed by a ball-on-disc tribometer using steel spheres as counterpart material. Friction coefficient was provided by the equipment, whereas wear rate was evaluated by the wear volume. Wear tracks on disc surfaces and worn cross-sections were analysed by means FEG-SEM, EDS measurements, XRD, roughness, and hardness tests. Bainitic microstructure offers better wear resistance compared to pearlitic-ferritic microstructure due to higher hardness, strain hardening capability, and strain-induced transformations. Adhesion and tribo-oxidational wear are the main wear mechanisms; the extent of oxidation increases increasing austempering temperature and it is maximum for samples treated at 350 °C and pearlitic-ferritic microstructure.

Keywords: carbide-free bainite, sliding wear, retained austenite, TRIP effect

1. Introduction

Over the last decades, several studies have been dedicated to the development of new bainitic steels whose composition is characterized by an interesting combination of tensile strength, ductility, and impact toughness [1–6]. In fact, as reported in the literature, these new steels can reach ultimate tensile strength (UTS) levels around 2 GPa, total elongations above 20%, and fracture toughness values around 100 MPa $m^{1/2}$ [7].

These steel grades, belonging to the 3rd generation of the advanced high-strength steels (AHSS), show a multiphase microstructure composed of carbide-free bainite with a significant volume fraction of stable carbon enriched retained austenite (RA) and martensite [8]. Such microstructure is obtained after austempering treatments. It consists of an austenitizing stage followed by rapid quenching and isothermal holding in a hot bath at a temperature between the bainite start (Bs) and martensite start (Ms) temperatures for a predetermined interval of time [9,10]. During the isothermal holding time, part of the austenite transforms into carbide-free bainite due to the presence of silicon and aluminum, which suppresses cementite precipitation [9,11]. Owing to the low solubility of carbon in ferrite, carbon is also rejected and enriches the austenite which becomes more stable and its retention at room temperature is favored [9]. An accurate alloy design guarantees low martensite start temperatures, which in turn allows performing isothermal treatments at very low temperatures, producing nanostructured bainite with excellent mechanical responses [3,12,13]. The addition of alloying elements, such as Cr, Mo, and V, in fact, could be added to refine the microstructure and modify Ms.

The main peculiarity of RA is its capability to undergo martensitic transformation when subjected to mechanical stresses, thus enhancing material tensile strength, ductility, and delaying necking [9]. This phenomenon is named Transformation-induced plasticity (TRIP) effect.

As a matter of fact, the stabilization of retained austenite at room temperature is of primary importance. Retained austenite stability depends on several factors: carbon content, grain size, temperature, and morphology [9,14–17]. Higher carbon content and lower grain size favor more stable RA. Some studies reported that two morphologies of RA in carbide-free bainitic steels can be distinguished: a) blocky-like and b) film-like retained austenite [8,9,18]. Blocky-like retained austenite is coarser and less rich in carbon in comparison with film-like retained austenite and mainly exists between the bainitic ferrite sheaves [19,20]. The blocky-like morphology contains many effective sites for martensitic nucleation and therefore higher is the driving force for the transformation. These characteristics make blocky-like retained austenite more prone to undergo martensitic transformation during loading in comparison with the film-like retained austenite [8,21]. Carbon in blocky-like RA is not homogenously distributed and martensitic transformation takes place at lower strain levels in grain regions with low carbon content. In contrast, the grain regions with higher carbon content only transform when the strain increases. On the other hand, film-like retained austenite is distributed between bainitic plates; moreover, it is the richest in carbon and it is characterized by the highest thermal and mechanical stability [22]. The large carbon enrichment, which can reach 2% [19],

leads to solution strengthening; this element is trapped at dislocation sites [23] that are active points for strain-induced martensite nucleation.

According to the literature [8,24,25], carbide-free bainitic steels are promising materials also for applications in which high wear resistance is required such as heavy rails, rolling-element bearings, and gears [26]. Guo et al. [24] highlighted the superior two-body wear resistance of bainitic steels in comparison with that of quenched and tempered (Q&T) steels. The authors demonstrated that the improved tribological properties of carbide-free bainitic steels derived from an ultrafine microstructure and a higher hardness, which are favorable against abrasion damage. Similarly, Sourmail et al. [25] and Wang [27] investigated the mechanical and tribological properties of high silicon and high carbon bainitic steels. Their main results included improved wear rates in comparison with those of quenched and tempered steels or standard lower bainitic steels (LB) thanks to the destabilization of retained austenite, especially below the worn surface, that leads to hardness increase and delay in defects nucleation and propagation.

A beneficial effect of small bainitic plates and high hardness on wear resistance was also reported by several authors. Yang et al. [24] and Mogdahham et al. [25] demonstrated that there is a proportional decrease in wear rate as isothermal treatment temperature decreases and as the microstructural refinement occurs. In fact, very fine microstructures show more resistance to the formation of a white etching layer (WEL) caused by severe and repeated plastic deformation.

Jin and Clayton compared the wear resistance of carbide-free bainite steel to that of standard pearlitic rail steel demonstrating the possibility to achieve the same or even better tribological performance while withstanding very large plastic deformations [30]. Accordingly, the same authors pointed out that the TRIP effect plays a role of primary importance. Leiro et al. [7] justified the higher wear resistance of bainitic steels considering the strong work hardening and the microstructural evolution under wear conditions. The authors demonstrated that martensite generated by the TRIP effect is harder than that formed during the final cooling of the heat treatment. The TRIP-induced martensite also produces compression stresses which represent an obstacle to crack propagation and reduce the wear rate.

Actually, the requirement from the industry regards new materials with high mechanical properties in order to reduce fuel consumption and costs and to improve the service life of the components. Thus, the investigation of new compositions is necessary, especially with a low amount of expensive alloying elements and with a carbon content that does not affect weldability. In this work, a newly designed steel with 0.38 % carbon and 3.2 % silicon was produced and isothermally treated at

temperatures of 250, 300, and 350 °C to obtain a carbide-free bainitic microstructure. In particular, the completely new composition was specifically designed to obtain low-cost, high-resistant steel with good weldability. The tribological behavior of this novel steel was for the first time studied in this paper in dry sliding conditions. The wear properties were compared with those of steels typical of heavy rails applications with the same chemical composition, but with a pearlitic-ferritic microstructure resulting from an annealing treatment. Microstructural changes after tribological tests and the main wear mechanisms were also investigated.

2. Experimental procedure

2.1 Alloy and heat treatment

The studied alloy, whose chemical composition is shown in **Table 1**, was produced by vacuum induction melting (VIM) in the form of an ingot of 50 kg starting from high purity raw material. As can be seen in **Table 1**, a large amount of silicon was added to the alloy to prevent cementite precipitation during isothermal treatments [31,32]. The ingot was reheated at 1200 °C and hot-rolled in seven passes to obtain a 20 mm thick plate. Cylindrical discs of 45 mm in diameter and 5 mm in thickness were then cut along the plate thickness and perpendicularly to the rolling direction, employing a wire electro-discharge machine (Sodick Europe Ltd., Warwickshire, United Kingdom).

The discs were subjected to different heat treatments (annealing and austempering), which were designed according to previous works performed by the authors [33]. Prior to heat treatments, the onset of martensitic transformation and austenitizing temperatures (Ac_1, Ac_3) were experimentally determined by dilatometry (DIL805A/D, TA Instrument, Hüllhorst, Germany) [34]. The Ms temperature was equal to 245 °C, whereas the Ac_1, and Ac_3 temperatures were 778 and 834 °C, respectively. A scheme of heat treatments carried out on the samples is depicted in **Figure 1**, whereas the details concerning the process parameters used during the heat treatments are resumed in **Table 2**. Annealing treatment was performed after austenitization, in a Fours H&C (Fours H&C, Fernelmont, Belgium) electrical muffle furnace at 900 °C, with a heating rate of 10 °C/s, 5 minutes holding time, and cooling inside the furnace until room temperature. Austempering of discs with carbide-free bainitic microstructure was conducted as follows: austenitization in the electrical muffle furnace under the same temperature, heating rate, and time conditions plus quenching in salt baths at 250, 300, and 350 °C. The discs were then held in the baths for a time sufficient for the completion of the bainitic transformation, and finally, water cooled to room temperature. During each stage of the heat treatments, the

temperature of specimens was monitored by a K thermocouple (Delta OHM, Selvazzano, Italy).

After the heat treatments, the samples were ground with fine SiC papers from grit size P320 to P2400, polished with clothes and diamond paste (6 and 1 μm) to minimize the surface roughness, and cleaned with ethanol.

Table 1 Chemical composition of the studied alloy (wt.%).

C	Si	Mn	Al	Cr	Ni	Mo	Cu	Fe
0.38	3.2	2.65	0.1	0.05	0.05	0.02	0.05	Balance

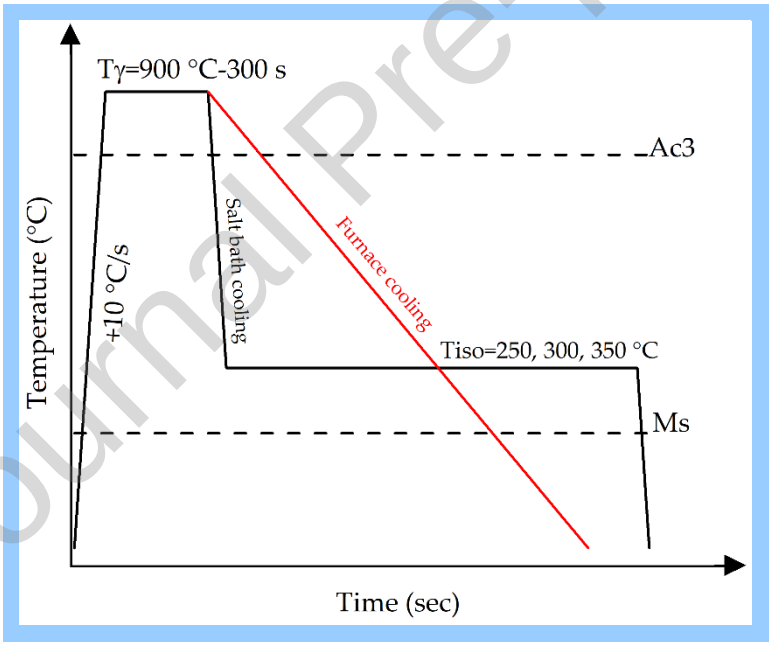

Figure 1 Scheme of the heat treatments carried out on the samples (red line is referred to the furnace cooling performed at the end of annealing treatment).

Table 2 Details concerning the process parameters used during heat treatments (T_γ = austenitizing temperature, t_γ = austenitizing time, T_{iso} = temperature of the salt bath, t_{iso}= soaking time in the salt bath).

Sample ID	T_γ (°C)	t_γ (min)	T_{iso} (°C)	t_{iso} (h)

250 °C	900	5	250	4.5
300 °C	900	5	300	2
350 °C	900	5	350	2.5
Annealed	900	5	-	-

2.2 Microstructural analysis

Standard metallographic techniques were employed for the preparation of the samples for microstructural analysis. Cross-sections (samples observed across the thickness of the metal) were obtained from the discs before and after wear tests by using the following procedure: a) cutting with SiC disks lubricated with a water-oil emulsion; b) mounting in conductive resin with graphite dispersed powder; c) grinding with SiC papers (320, 500, 800 and 1200 grit); d) polishing with clothes and diamond polycrystalline suspensions (6, 3 and 1 μm); etching with Nital 2 (2% nitric acid and 98% ethanol) solution.

A Leica Cambridge Stereoscan LEO 440 (Leica Microsystems S.r.l., Milan, Italy) scanning electron microscope (SEM) and a Zeiss ULTRA 55 (Zeiss, Oberkochen, Germany) scanning electron microscope with high-resolution Schottky field emission gun (FEG-SEM) were used for microstructural observations on all heat-treated samples. For microstructural analysis of carbide-free bainitic specimens, a Philips CM30 (Philips, Amsterdam, Netherland) transmission electron microscope (TEM) was also adopted, operating at 300 kV acceleration voltage.

2.3 X-ray diffraction (XRD)

Phase identification and quantification were carried out by a Siemens D500 X-Ray diffractometer (Siemens, Munich, Germany), with Cu Kα (and Kβ filtered) radiation tube, a 40 kV voltage, a 30 mA filament current, and a pattern acquisition from 40° to 105° (2θ mode, 0.025° step scan, 3 s/step scanner velocity). Rietveld analysis was performed through Maud software (Version 2.96) [35] to calculate the volume fraction of retained austenite, amount of carbon in retained austenite, and austenite lattice parameter. Especially, the amount of carbon in retained austenite was determined using the following equation proposed by Dyson and Holmes [36]

$$a_\gamma = 3.5780 + 0.033w_C + 0.00095w_{Mn} - 0.0002w_{Ni} + 0.0006w_{Cr} + 0.0056w_{Al} + 0.0031w_{Mo} + 0.0018w_V \quad \text{(Eq. 1)}$$

where w_i stands for the weight percent of the element i and a_γ is the austenite lattice parameter in Å. Prior to wear tests, the measurements were conducted in the center of the specimens. In agreement with the procedure described in [37], for avoiding the impact of the grinding operation, the preparation of XRD samples included cycles of etching and polishing to remove any deformed layer that could be formed during the grinding step. After wear tests, XRD measurements were carried out directly on the wear tracks.

2.4 Microhardness tests

Microhardness examinations were performed before and after wear tests by an EMCO DuraScan G5 (EMCO-TEST Prüfmaschinen GmbH, Kuchl, Austria) Vickers microhardness tester, with an applied load of 0.3 kg and a dwell time of 15 s. Each microhardness value is an average of 20 measurements. Microhardness profiles were also carried out on the cross-section of the worn specimens with a load of 0.05 kg and starting from three different points under the worn surfaces. The minimum distance between two consecutive indentations was at least three times the diagonal length.

2.5 Wear tests

Wear tests were performed by a TR20LE tribometer (Ducom Instrument, Bengaluru, India) in ball-on-disk configuration, under dry sliding conditions, and at room temperature, in accordance with the ASTM G99-17 standard [38]. Balls made of 100Cr6 steel 6 mm in diameter were used as counterpart material. During experiments, discs were rotating while balls were pressed against them by dead weight loading and lever systems. The tribometer was also equipped with a load cell for frictional force measurement, an encoder for the control of the rotational speed, and a linear variable differential transformer (LVDT) sensor for wear evaluation. During the tests, the coefficient of friction (COF) was directly calculated by the equipment. Wear tests were conducted under a normal load of 20 N, at a sliding speed of 0.3 m/s and for a sliding distance of 2000 m. Three wear tests were carried out for each heat treatment conditions. Specific wear rate (SWR) of discs, expressed in mm^3/Nm, was calculated according to Eq. 2 by measuring the cross-section area of the wear track with a Talysurf CCI-Lite non-contact 3D profilometer (Taylor-Hobson, Leicester, UK). Each area value, as an average of four measurements of cross-section areas along the track, was used to determine the wear volume:

$$SWR = \frac{\Delta V}{LD} \quad \text{(Eq. 2)}$$

where ΔV is the wear volume (mm^3), L is the applied load (N) and D is the sliding distance (m).

The surface topography of the worn surfaces was investigated by the same profilometer and the arithmetical mean height of the surface (Sa) was evaluated. Four readings were acquired at four different locations for each sample. The obtained results were then compared with the values of Sa achieved before wear tests.

In order to identify the main wear mechanisms, the wear tracks on discs were observed by a Zeiss EVO MA 15 (Zeiss) scanning electron microscope equipped with an Oxford X-Max 50 (Oxford Instruments, Abingdon-on-Thames, UK) energy dispersive microprobe for semi-quantitative analyses (EDS). The SEM micrographs were recorded in secondary electron imaging (SEI-SEM) and back-scattered electron (BSE-SEM) mode. Finally, the cross-sections of worn samples were investigated by the same FEG-SEM microscope to identify the microstructural changes induced by the sliding motion between the mating materials.

3 Results and discussion

3.1 Microstructural characterization

The microstructures observed on the cross-section of the heat-treated samples before wear tests are depicted in **Figure 2**. After austempering at 250 °C, the samples show a fine carbide-free bainitic microstructure. Scanning electron microscopy allowed the detection of the presence of bainitic ferrite alternated with film-like and blocky-like retained austenite (**Figure 2a**). Blocky-like retained austenite shows a micrometric size, while the film-like retained austenite sizes in the range of sub-micron. Sub-units of coalesced bainite are also observed in the microstructure, because of sub-units growth with the same crystallographic orientation [39]. As a result of increasing the isothermal treatment temperature (300 and 350 °C), a coarser carbide-free bainitic microstructure is formed (**Figure 2b,c**). In agreement with the literature [12,34,40], a comparison between the SEM micrographs in **Figures 2a-c** reveals that a finer microstructure is obtained at the lowest temperature for the bainitic reaction. Microstructural refinement is connected with the higher driving force for nucleation rate of bainitic ferrite, strength of undercooled austenite and impingement of newly formed sub-units achieved when the transformation temperature is lowered [41]. In addition, contrary to samples treated at 250 °C and 300 °C, martensite (α') is also present in the microstructure of specimens treated at 350 °C, as demonstrated by the

authors in previous studies [34]. Finally, in Figures 2e,f, the FEG-SEM and TEM micrographs at high magnifications highlight the absence of cementite in bainitic ferrite, thus confirming the effective capability of silicon to avoid carbide precipitation [3].

After annealing, the specimens exhibit the typical microstructure of annealed hypoeutectoid steels, consisting of pearlite and primary ferrite (Figure 2d). The high amount of pearlite with respect to primary ferrite is due to the shift of the eutectoid point induced by the high contents of silicon and manganese added to the alloy [42].

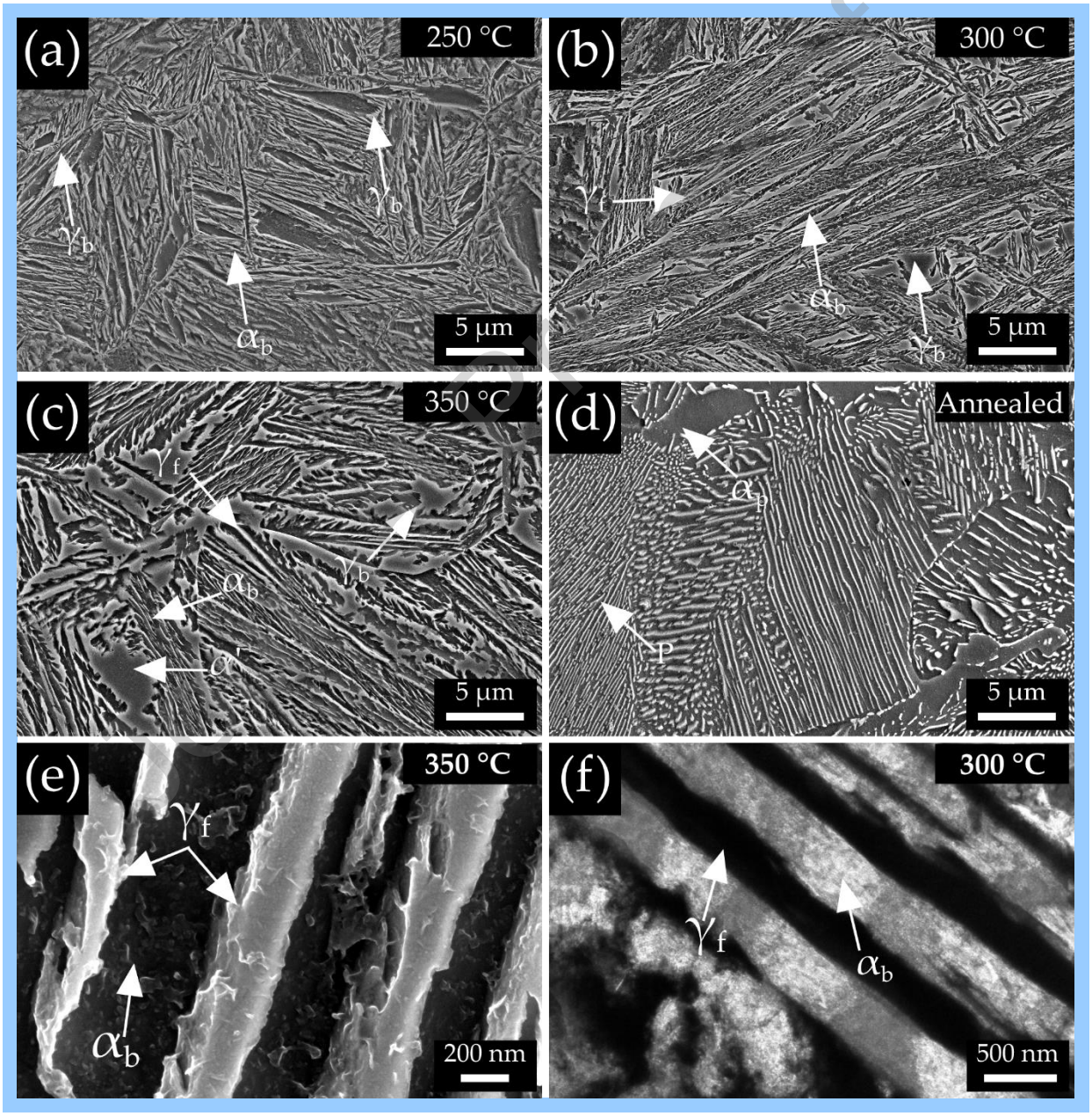

Figure 2 (a-e) FEG-SEM micrographs of the microstructure observed on the cross-section of the heat-treated samples before wear tests showing, in the order, the microstructure after austempering at 250 °C consisting of bainitic ferrite (α_b), film-like retained austenite (γ_f) and

blocky-like retained austenite (γ_b), the same microstructure after austempering at 300 and 350 °C, with also martensite (α'), the pearlitic-ferritic microstructure after annealing (P: pearlite, α_P: primary ferrite), and details of the absence of cementite in bainitic ferrite detected in austempered samples. (f) TEM micrograph of the specimens austempered at 300 °C further confirming the effective capability of silicon to avoid carbide precipitation.

3.2 Bulk microhardness

The mean values ± standard deviations of bulk microhardness (HV0.3) of all samples before wear tests are presented in **Table 3**. As can be seen in the table, the mean bulk microhardness increases as the isothermal treatment temperature decreases. This increase may be attributed to the microstructural refinement and the increase in dislocation densities reached at lower transformation temperatures [12,37]. During bainitic transformation, sessile dislocations are formed due to the interaction of glissile dislocations at the slip planes [44], newly introduced sessile dislocations lead to hardness increase, strength, and resistance to plastic deformation [44,45]. As the isothermal treatment temperature increases, dynamic recovery can occur and the annihilation processes lead to a reduction in dislocation density [44]. Furthermore, thanks to the microstructural refinement achieved at a lower temperature for bainitic reaction, higher strength and hardness are possible due to the strengthening of the lath boundary [44].

Table 3 Mean values ± standard deviations of bulk microhardness (HV0.3) of all samples before wear tests.

Sample ID	**$HV_{0.3}$**
250 °C	561 ± 8
300 °C	494 ± 5
350 °C	458 ± 8
Annealed	310 ± 10

3.3 XRD analysis

The X-ray diffraction patterns of specimens after heat treatment are shown in **Figure 3**, while the volume fraction of retained austenite, amount of carbon in retained austenite, and austenite lattice parameter for all samples in the same conditions and as determined by Rietveld analysis are presented in **Table 4**. The XRD patterns of annealed samples show the main reflections of α-iron (associated with bainitic ferrite), together with a number of minor reflections of γ-iron (associated with retained austenite). Decreasing in isothermal treatment temperature corresponds to an increase in the bainitic reaction rate; accordingly, an increase in bainitic ferrite content is observed. By lowering the isothermal treatment temperature, the amount of retained austenite also decreases, and its carbon content increases, in agreement with the general T0 curve, that determines the maximum carbon enrichment and degree of transformation possible at each isothermal transformation temperature, reported by Bhadeshia [41]. These results are comparable to those previously reported for austempered carbide-free bainitic steels [18,40,41]. In fact, several authors demonstrated that as the austenite supercooling increases, the bainite nucleation rate increases [34]. Irrespective of type of the heat treatment, the absence of cementite peaks also confirms the role of silicon in suppressing precipitation of this microstructural constituent, as supported by the microstructural observations through scanning and transmission electron microscopy. Concerning annealed samples, only reflections of α-iron (associated with ferrite) are visible in **Figure 3**.

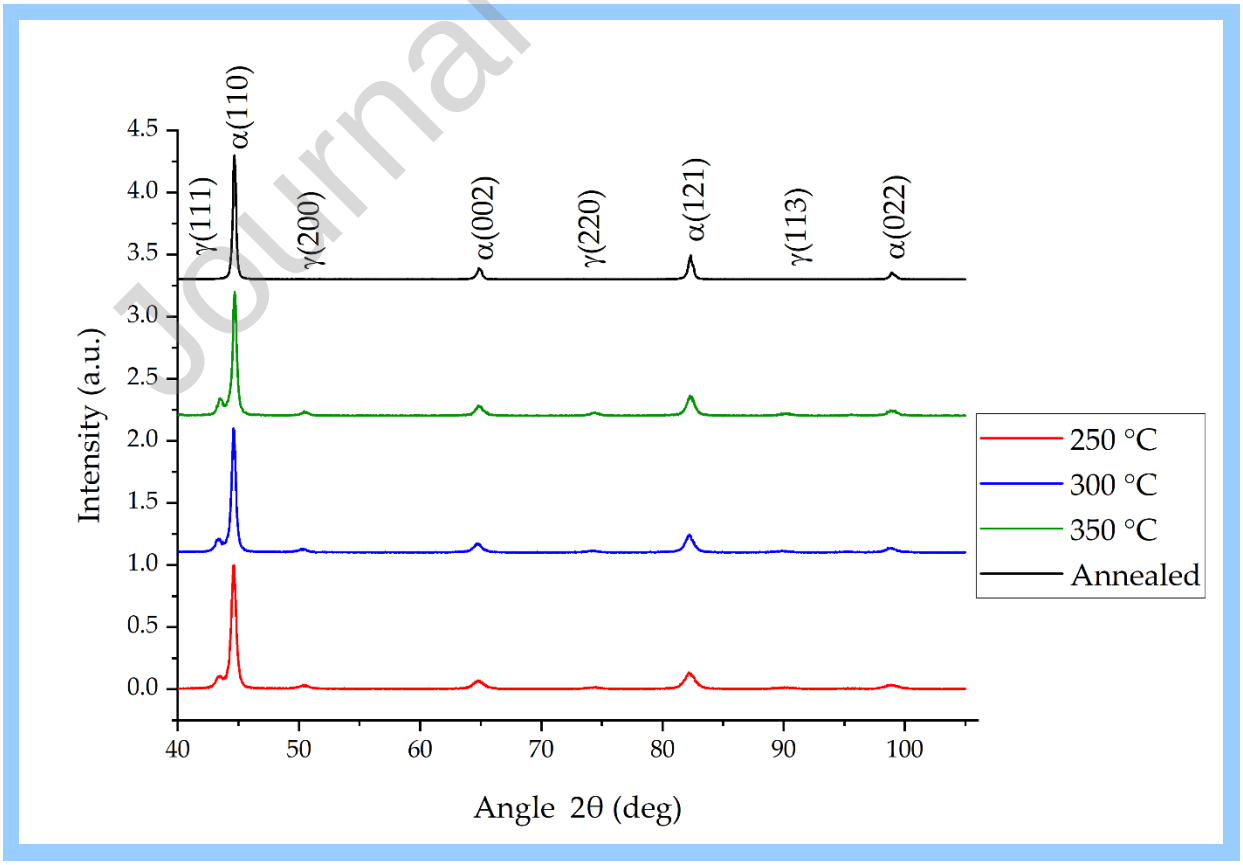

Figure 3 X-ray diffraction patterns of all specimens after heat treatment.

Table 4 Mean values ± standard deviations of volume fraction of retained austenite (Vγ), amount of carbon in retained austenite (Xγ), and austenite lattice parameter (aγ) for all samples after heat treatment, as determined by Rietveld analysis.

Sample ID	Vγ (%)	Xγ (wt.%)	aγ (Å)
250 °C	12 ± 3	1.20±0.04	3.623±0.002
300 °C	14 ± 3	1.11±0.04	3.619±0.002
350 °C	16 ± 3	0.87±0.04	3.607±0.002
Annealed	-	-	-

3.4 Wear data

3.4.1 COF and wear rate

The coefficient of friction variations with sliding distance together with the mean values ± standard deviations of coefficient of friction at the steady state for all heat-treated samples are depicted in **Figure 4**. All curves show a running-in period (up to a sliding distance of about 250 m), during which the COF sharply increases probably due to the low contact surface area. In fact, at the beginning of the tests this area corresponds to discrete points (i.e., asperities) of the mating surfaces; accordingly, the load per area unit is very high. During sliding motion, the asperities are removed and the contact area increases [7,43-46]. As reported by some authors [45], the duration of the running-in period depends on the surface finishing and the chemical compositions of both the material before wear tests and the counter-body. It especially increases with increasing surface roughness. In this work, all specimens were characterized by the same finishing, therefore, the duration of the running-in period is almost independent of the heat treatment conditions. After this period, the coefficient of friction reaches a steady state, but the values fluctuate until the end of the tests (mostly in the case of annealed samples). This is may be linked to the occurrence of adhesive wear. Formation and fracture of adhesive junctions and the removal of transfer particles at the contact surfaces can induce rise and fall of the

frictional force which, in turn, can lead to peaks and local variations in the COF values [43].

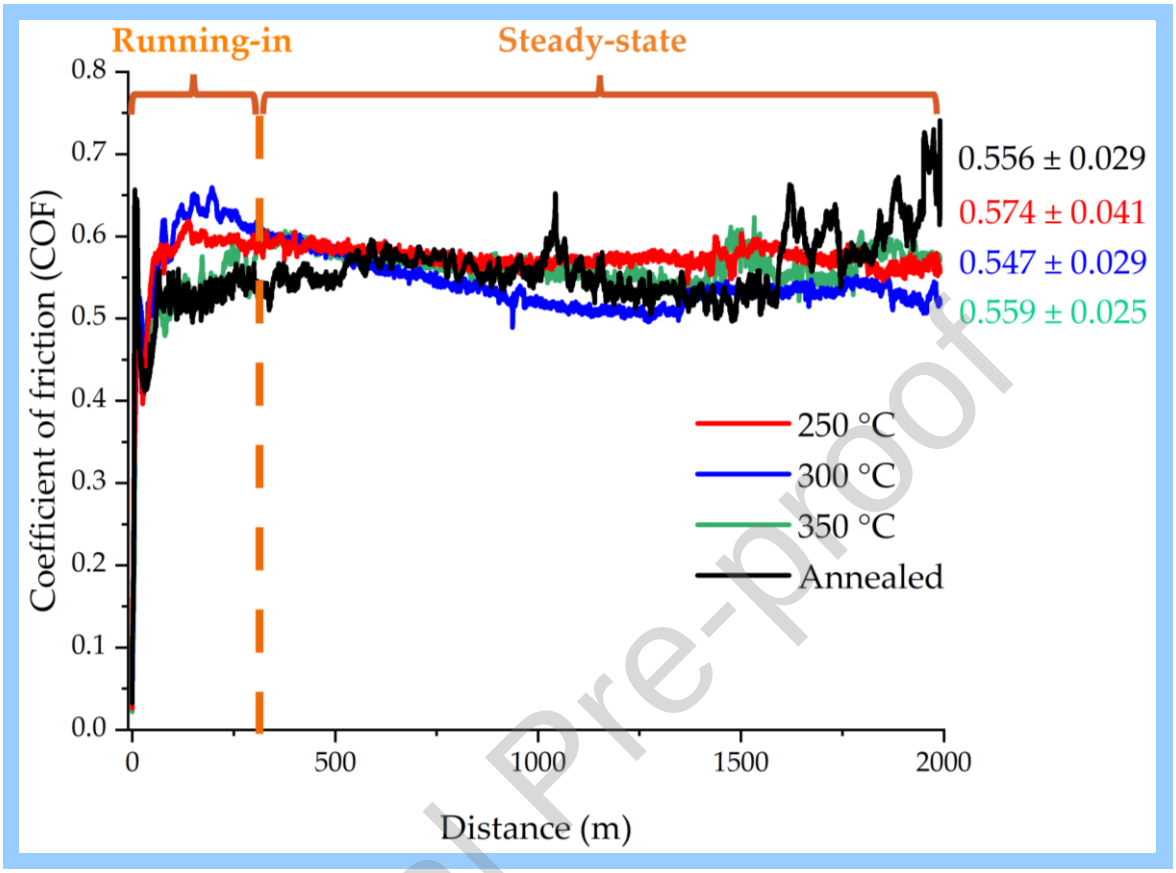

Figure 4 COF variations with sliding distance together with the mean values ± standard deviations of coefficient of friction at the steady state for all heat-treated samples.

As can be seen in Figure 4, the mean coefficient of friction at the steady state is not influenced by the microstructure before wear tests, with all mean values falling within a range between 0.547 and 0.574. These values are similar to those previously reported in [47]. However, the tribological behavior of the steel examined is affected by the microstructure after heat treatment, it can be demonstrated that the wear resistance is strictly linked to the initial microstructure, from which the original hardness derives and to the microstructural changes and mechanical properties of the portions of material close to the wear surfaces.

The mean specific wear rates for all heat-treated samples are shown in Figure 5. Considering austempered samples, the mean SWR increases with increasing isothermal treatment temperature from 7.82E-05 to 1.68E-04 $mm^3/(Nm)$. Therefore, as demonstrated in Subsection 3.4.3, the carbide-free bainitic microstructure with the lowest content of retained austenite and the highest amount of carbon in retained austenite (as a stabilizing element of this phase) exhibits the best wear performance.

Finally, the mean specific wear rate of pearlitic-ferritic specimens is the highest and equal to 7.09E-04 $mm^3/(Nm)$.

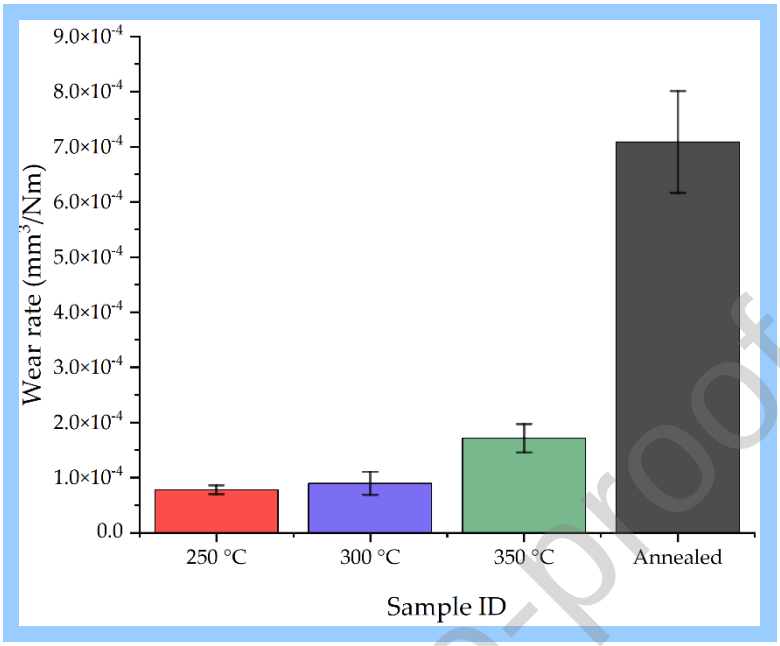

Figure 5 Mean specific wear rates for all heat-treated samples (error bars represent standard deviation).

3.4.2 Analysis of the worn surfaces

In Table 5, the mean values ± standard deviations of the arithmetical mean height of the surface (Sa) for all heat-treated samples before and after wear tests are listed. Before wear tests, the surface roughness of the specimens is similar and consistent with the finishing procedure employed for the preparation of the discs. Irrespective of the type of heat treatment, Sa increases after wear tests. The final mean values of the arithmetical mean height of the surface are maximum for annealed samples and between 0.741 and 1.169 μm for the austempered ones.

Table 5 Mean values ± standard deviations of the arithmetical mean height of the surface (Sa) for all heat-treated samples before and after wear tests.

Sample ID	Sa (μm)	
	Before wear	**After wear**
250 °C	0.053 ± 0.006	0.851 ± 0.247

300 °C	0.032 ± 0.014	0.741 ± 0.332
350 °C	0.041 ± 0.007	1.169 ± 0.369
Annealed	0.048 ± 0.006	2.665 ± 0.476

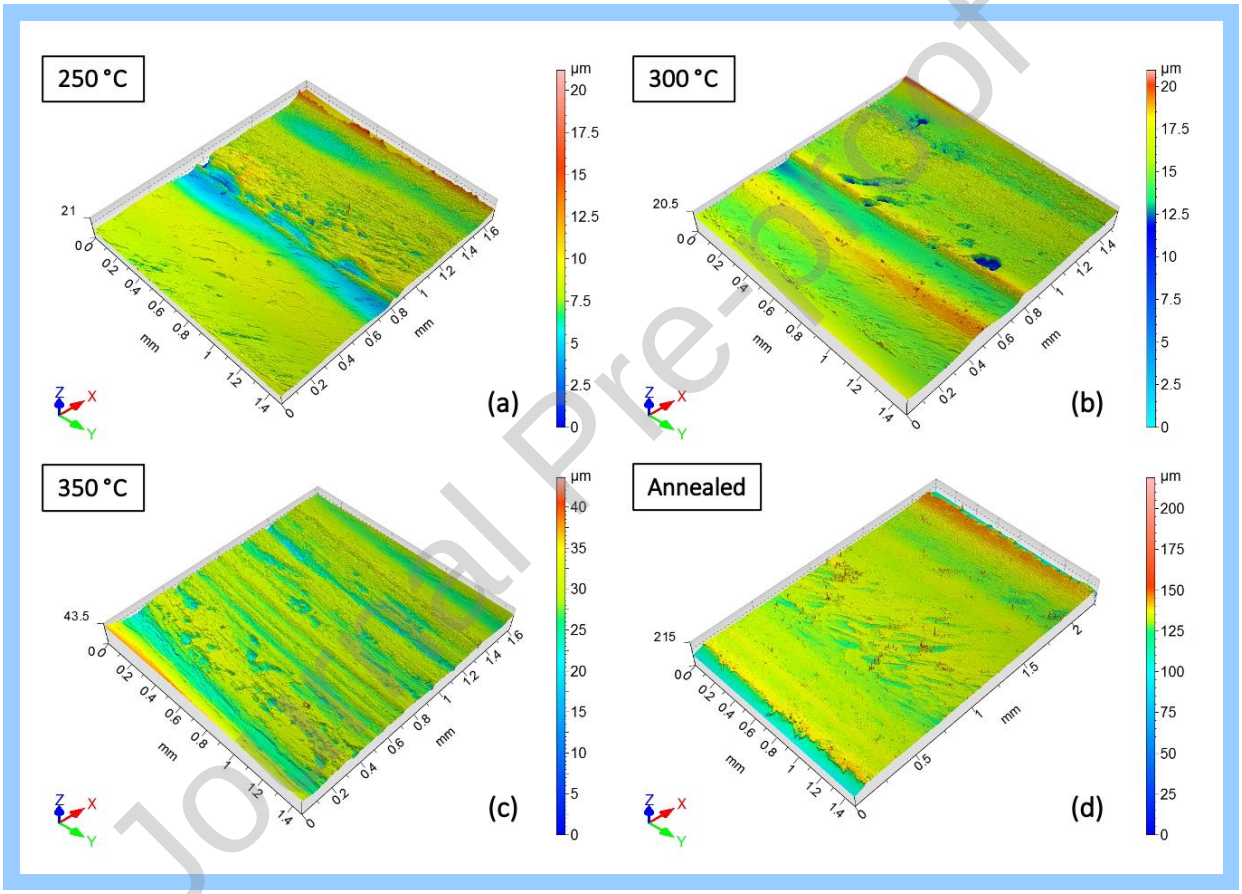

Figure 6 The 3D isometric views of the wear tracks observed on the discs: (a) austempered at 250 °C; (b) austempered at 300 °C; (c) austempered at 350 °C; (d) annealed.

Examples of 3D surface textures of the worn surfaces of all heat-treated discs are shown as 3D isometric views in Figure 6a–d. All wear tracks mainly consist of deep scratches and coarse grooves. The worn surfaces of samples austempered at 250 °C appear slightly smoother than those of the other heat-treated specimens. A certain amount of metal transfer can also be detected on the wear tracks of all discs, especially on one edge of the tracks of annealed samples.

The SEI-SEM micrographs of the wear tracks observed on the heat-treated discs are reported in **Figure 7**. In all cases, the morphology of worn surfaces suggests that adhesion and tribo-oxidational wear are both active during sliding motion. For most steels, oxidation of the asperities takes place due to the reaction with oxygen in the atmosphere, thus generating a thin layer of native iron oxide on fresh surfaces [49]. When the load is applied, this oxide fractures, and new metal is available for the development of strong adhesive junctions at the contact interfaces. During sliding motion, these junctions are subjected to plastic deformation, compressive and tangential shear stresses. The slip of adhesive bonds may, therefore, occurs and shear bands can form on the worn surfaces [50]. The initiation and propagation of cracks provoked by the inability of the material in accommodating further plastic deformation then induce the generation of scale-like shear fractures similar to those visible in Figure 8a. These fractures are an index of metal transfer between mating surfaces [51]. The tribolayer can be retained on the wear track, undergoing work hardening and severe oxidation, until it reaches a critical thickness. Then it spalls off in the form of wear debris [49]. The created wear particles may be embedded into one of the surfaces, resulting in two-body abrasive wear; alternatively, the same particles can freely move between the surfaces, causing three-body abrasive wear [44]. Especially, the appearance of deep scratches and coarse grooves on the wear tracks (**Figure 8b**), already detected by non-contact 3D profilometry (**Figure 6**), supports the occurrence of these latter wear mechanisms. The fluctuations of coefficient of friction with sliding distance in Figure 4, together with the observed metal transfer, scratches, and grooves on the wear tracks also support the hypothesis that adhesion is one of the main wear mechanisms. The wear debris may lastly experience deformation and fragmentation. As a result, smaller wear particles with high surface energy are generated and readily oxidized [49]. The compression stresses in the contact zone favor agglomeration of these particles and the formation of the powdery wear debris observed in **Figure 8c**. Comparing the micrographs in **Figure 7**, it can be pointed out that the width of the wear tracks on samples austempered at 250 °C is the lowest. This confirms the best tribological performance displayed by the specimens heat-treated at the lowest isothermal treatment temperature. Moreover, the amount of material build-up is maximum for annealed samples and preferentially located at one edge of the wear track (details in Figure 8d), as already detected by non-contact 3D profilometry.

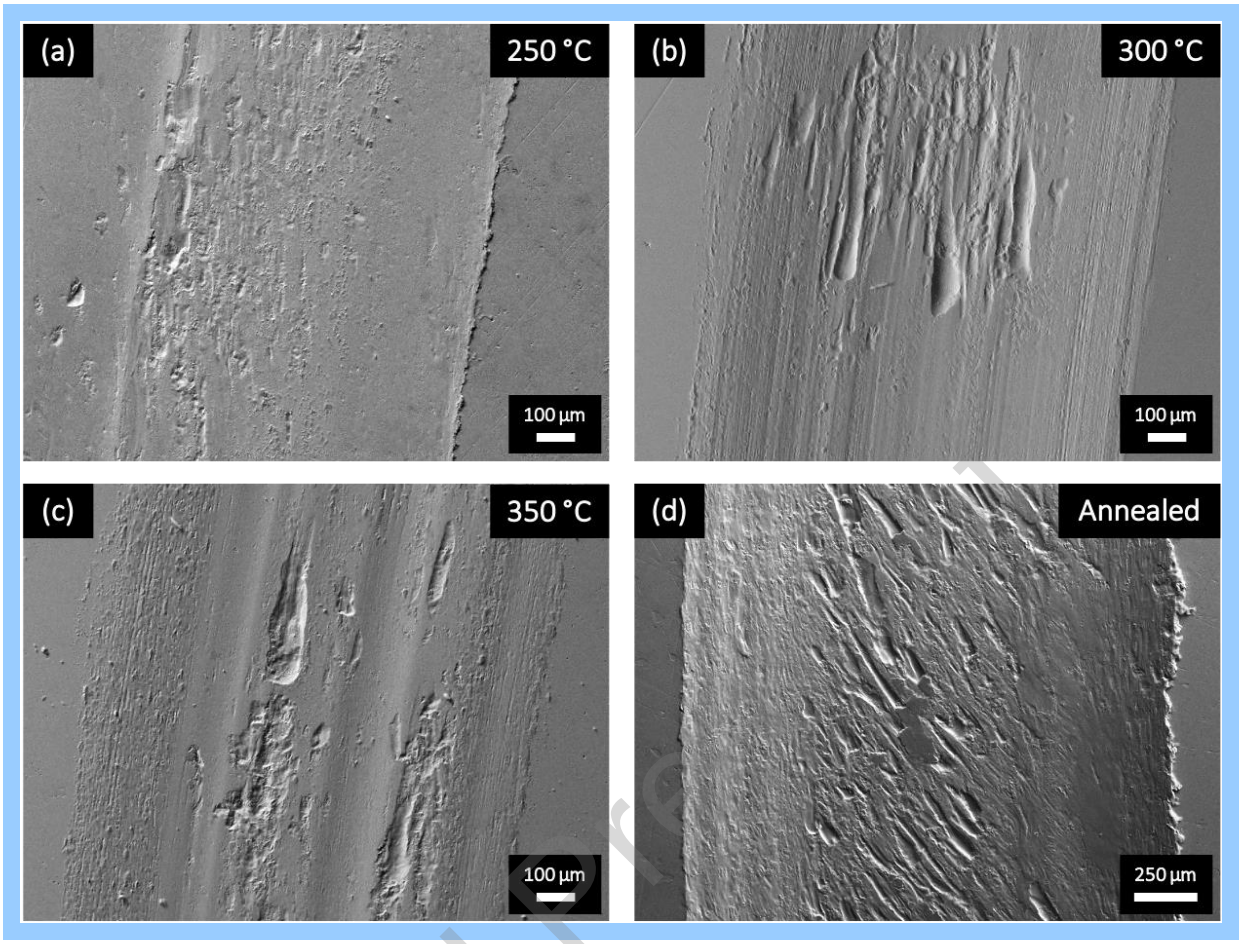

Figure 7 SEI-SEM micrographs of the wear tracks observed on the discs: (a) austempered at 250 °C; (b) austempered at 300 °C; (c) austempered at 350 °C; (d) annealed.

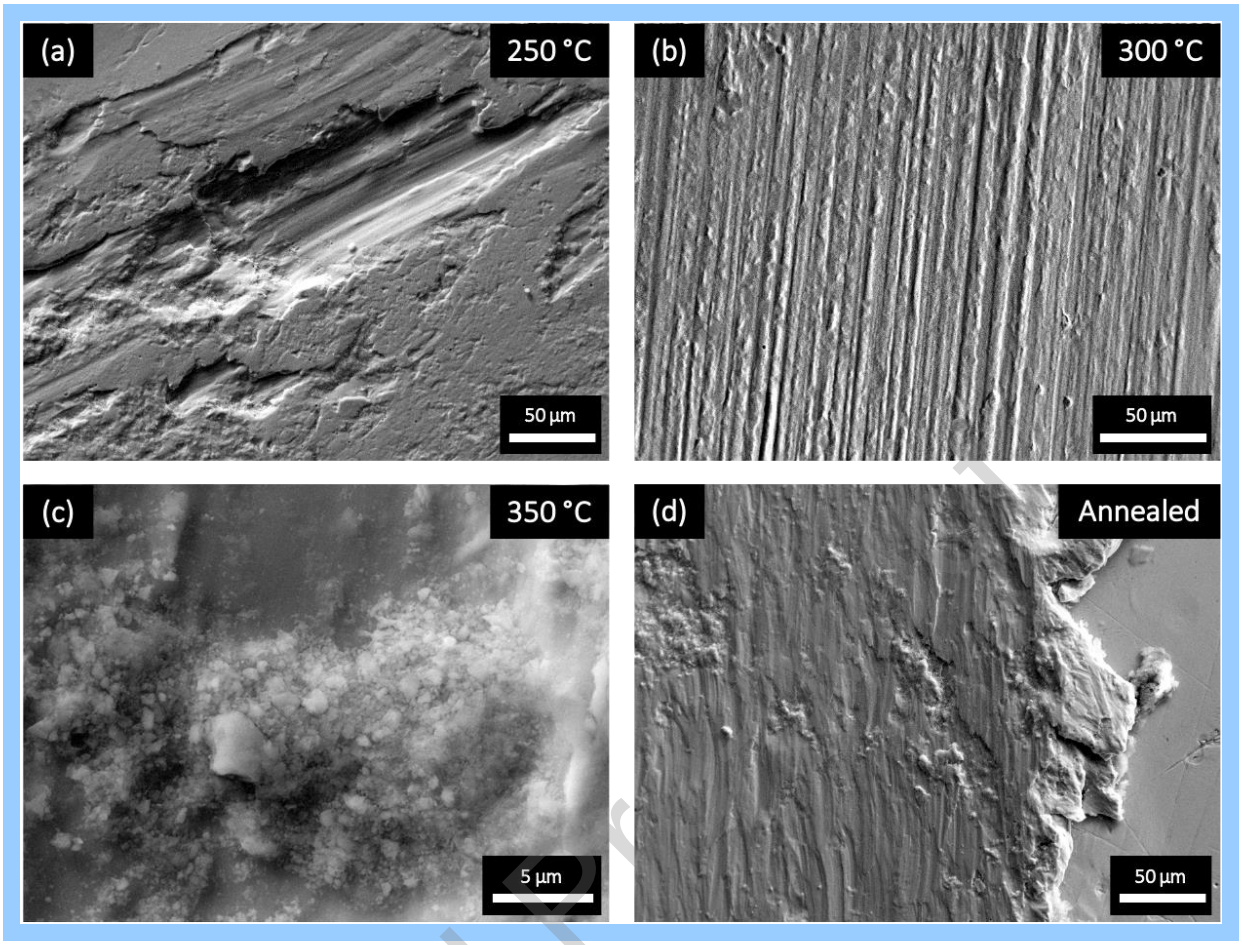

Figure 8 SEI-SEM micrographs of some details observed on the wear tracks of heat-treated discs: (a) scale-like shear fracture on samples austempered at 250 °C; (b) deep scratches and coarse grooves on specimens austempered at 300 °C; (c) powdery wear debris on samples austempered at 350 °C; (d) material build-up at one edge of the tracks on annealed specimens.

The SEM/EDS mapping of elemental distribution on the wear tracks of heat-treated samples is depicted in Figure 9. The EDS maps confirm the presence of metal transfer and oxidized wear debris on the worn surfaces. For the austempered specimens, the extent of oxidation increases with increasing the isothermal treatment temperature. In agreement with previous research [51], lowering this temperature refines the microstructure and increases the boundaries between grains and the number of defects (i.e., the areas with high surface energy). Accordingly, adhesion is promoted. Finally, the amount of oxidation on annealed samples is similar to that achieved on discs austempered at 350 °C.

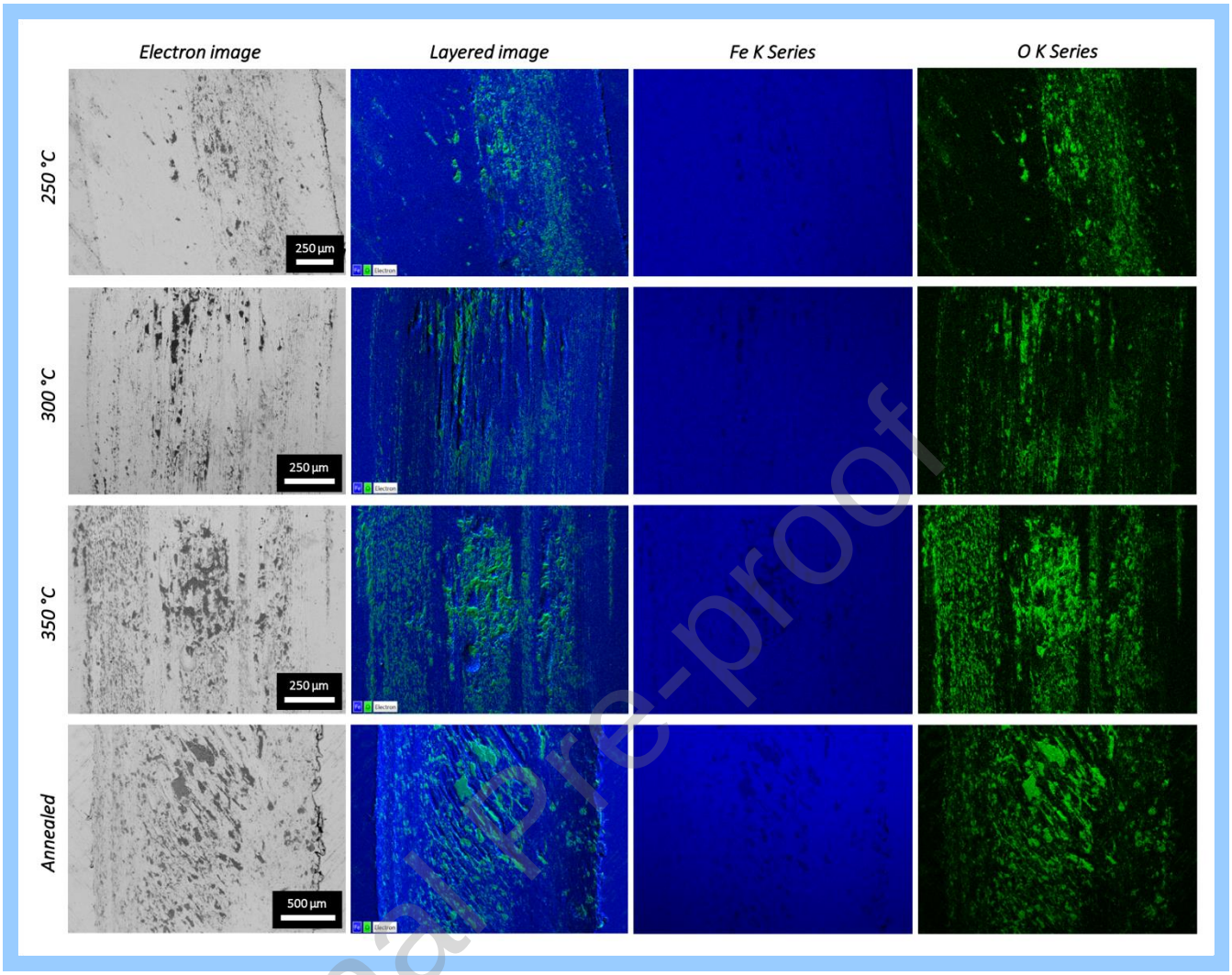

Figure 9 From the left: BSE-SEM micrographs of the wear tracks observed on the heat-treated discs; layered images of X-ray maps and maps of the elemental distribution of iron and oxygen on the same tracks.

3.4.3 XRD on wear tracks

The X-ray diffraction patterns of all specimens after wear tests are shown in Figure 10, whereas comparison between peaks of different crystallographic planes (γ{111} and α{110}) of austempered samples before and after wear tests is reported in Figure 11. Considering austempered samples, after wear tests the intensity of the peaks related to retained austenite is decreased, thus suggesting the occurrence of martensitic transformation during sliding motion against the counterbody (Figure 10). Nevertheless, it is not possible to discriminate martensite peaks from those attributed to bainitic ferrite due to low angle separation (Figure 11) [52]. Concerning annealed samples, no major changes in diffraction patterns are detected after wear tests.

Mean values ± standard deviations of volume fraction of retained austenite (Vγ) in worn austempered samples together with the percentage reduction of the same parameter (ΔVγ) after wear tests, as determined by Rietveld analysis, are reported in Table 6. According to Rietveld analysis, more than 60 % of retained austenite transforms into martensite during wear tests. In addition, the specimens austempered at 250 °C, showing the best tribological performance in terms of wear rate, exhibit the most stable retained austenite, as confirmed by the lowest value of ΔVγ. In agreement with the literature, the high work hardening capability and stability of RA lead to the best wear response [51–54].

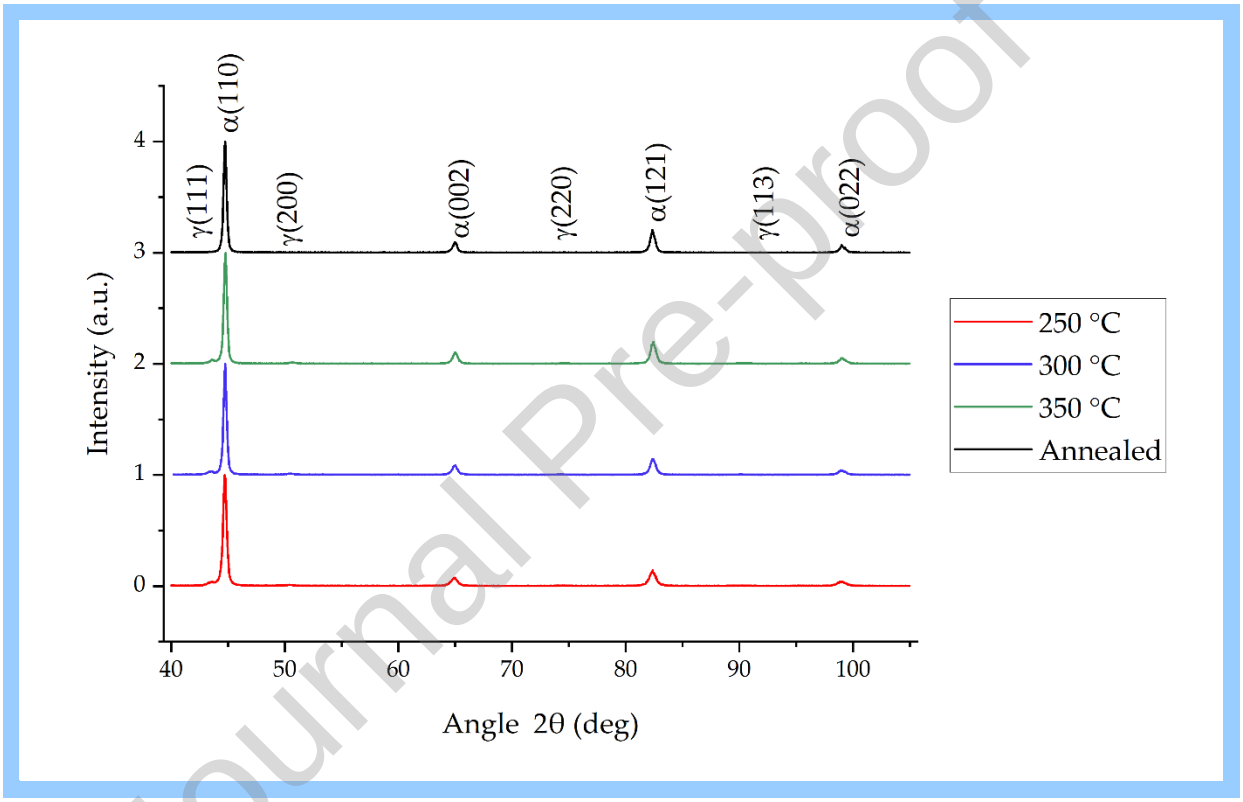

Figure 10 X-ray diffraction patterns of all specimens after wear test.

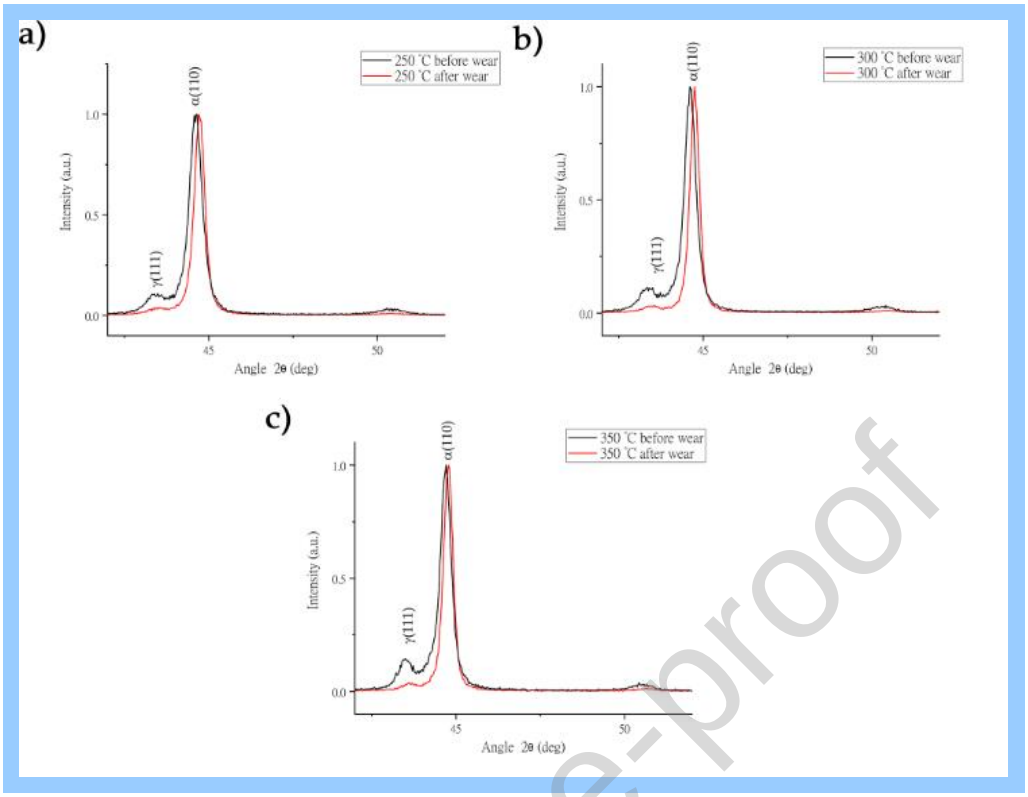

Figure 11 Comparison between peaks of different crystallographic planes (γ{111} and α{110}) of samples austempered at 250 °C (a), 300 °C (b), and 350 °C (c) before and after wear tests.

Table 6 Mean values ± standard deviations of volume fraction of retained austenite (Vγ) in worn austempered samples together with percentage reduction of the same parameter (ΔVγ) after wear tests, as determined by Rietveld analysis. The results come from the comparison with those in **Table 4**.

Sample ID	Vγ (%)	ΔVγ (%)
250 °C	4± 3	67 %
300 °C	5 ± 3	64 %
350 °C	5 ± 3	68 %

3.4.4. Microstructural analysis of worn cross-sections

The SEM micrographs of the microstructure observed on the cross-section of the austempered samples before and after wear tests are shown in **Figure 12**. In agreement with results previously reported in the literature [44,53], three different zones can be recognized in the sub-surface regions of all discs (**Figure 12b**, **e,** and **h**). Starting from the worn surface, there is a heavy plastically deformed and oxidized layer (zone A), whose thickness increases with increasing the austempering temperature from 250 to 350 °C. In this zone, the alignment of microstructural constituents along the counter body sliding direction is also visible, together with the fragmentation of bainitic ferrite (**Figure 12c**, **f,** and **i**). No cracks are detected in zone A of the specimens austempered at 250, 300, and 350 °C, evidencing the ability of carbide-free bainitic microstructures in accommodating severe plastic deformations and preventing crack initiation and propagation below the worn surfaces [53]. This is may be due to the barrier effect exerted by the high plastic stability of retained austenite and by the numerous interfaces between bainitic ferrite and retained austenite, which can hinder the mobility of dislocations, nucleation and propagation of cracks [55]. At higher magnification, non-etched portions of material are observed very close to the worn surfaces of discs austempered at 250 and 300 °C (**Figure 12c and f**). The presence of these featureless areas, probably deriving from the strain-induced transformation of retained austenite into martensite (TRIP effect), may support the results of X-ray diffraction measurements performed on the wear tracks, where significant reductions of the volume fraction of retained austenite are found. As pointed out by Chang [26], the non-etched regions are also responsible for the superior tribological performance of carbide-free bainitic samples, thanks to the formation of a hard phase and the introduction of crystallographic defects inside the material. Furthermore, the effect of silicon in preventing carbide precipitation reduces the probability of nucleation of defects, so long as they are sites of stress concentration.

In zone A of discs austempered at 350 °C, spallation occurs and some pits appear over the wear tracks (**Figure 12i**). The weakness of the coarse microstructure of these specimens is also highlighted by the presence of several micro-voids uniformly distributed below in the sub-surface regions. For samples heat-treated at 350 °C, strength of the material is limited in comparison with that of samples austempered at 250 and 300 °C, thus the microstructure is more prone to present defects. Thicker bainitic ferrite plates, combined with coarser and less stable retained austenite affects the tribological performance of steel [9]. In all austempered samples, a zone B is then individuated. This zone is characterized by a plastically deformed microstructure, once again oriented along the counter body sliding direction. Finally, the Zone C corresponds to the unaffected bulk material. A schematic illustration of the layered

microstructure highlighted on the cross-section of carbide-free bainitic steel after wear tests is reported in Figure 13.

The SEM micrographs of the microstructure observed on the cross-section of the annealed samples before and after wear tests are shown in **Figure 14**. The scanning electron microscope examinations revealed that the extent of severe plastic deformation is maximum for pearlitic-ferritic microstructure (**Figure 14b**). A higher number of shallow pits (due to the spallation occurrence), primary and secondary cracks nearly parallel to the worn surface and fragmentation of cementite lamellas are observed in the sub-surface regions close to the wear tracks (white, red, and green arrows in **Figure 14b**, respectively). Defects in **Figure 14b** and **c** suggest the triggering of fatigue phenomena during wear tests, as also proposed by Neong et al. [56]. In **Figure 14b**, non-etched portions of material are identified very close to the worn surfaces of discs. These regions probably result from localized austenitization and subsequent cooling that lead to the formation of martensite [57]. As for the austempered specimens, a plastically deformed zone with cracks inside ferritic grains (Figure 14d) and the unaffected bulk material are then individuated at a certain distance from the worn surfaces.

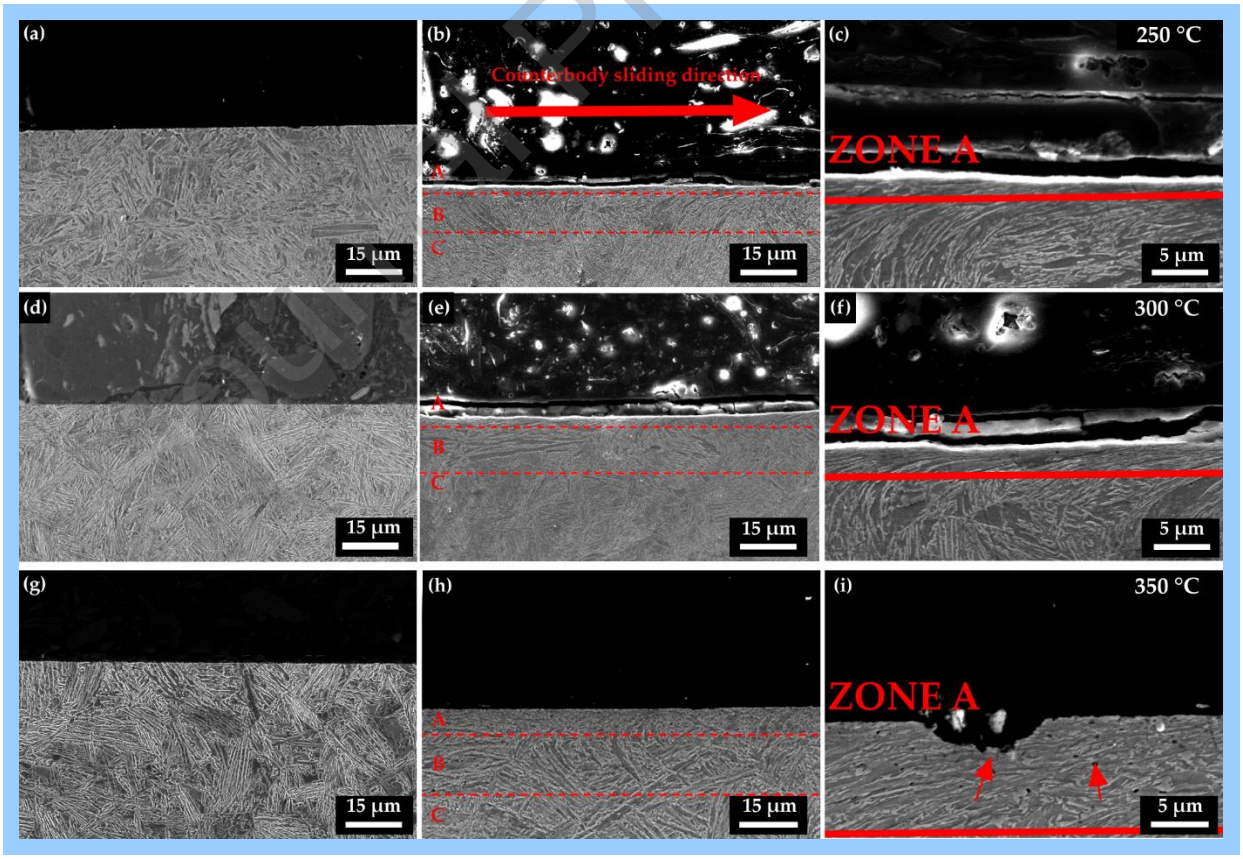

Figure 12 FEG-SEM micrographs of the microstructure observed on the cross-section of the austempered samples, before (a,d,g) and after wear tests. (b,e,h) Overview of the layered sub-surfaces. The red dashed lines indicate the boundaries between layers. From top to

bottom: heavy plastically deformed and oxidized zone (A), plastically deformed material (B), bulk material (C). The red arrow in (b) shows the counterbody sliding direction. (c,f,i) Details of zone A detected in the same samples. The red arrows in (i) evidence some pits and microvoids in the specimens austempered at 350 °C.

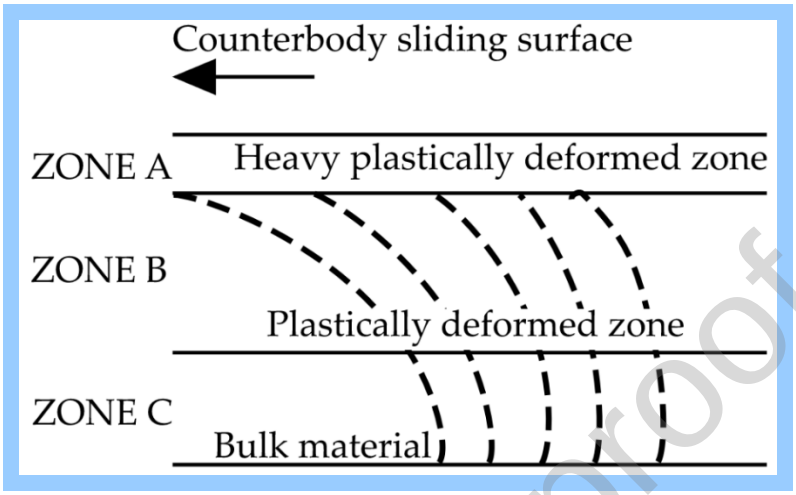

Figure 13 Schematic illustration of the layered microstructure highlighted on the cross-section of carbide-free bainitic steels after wear tests.

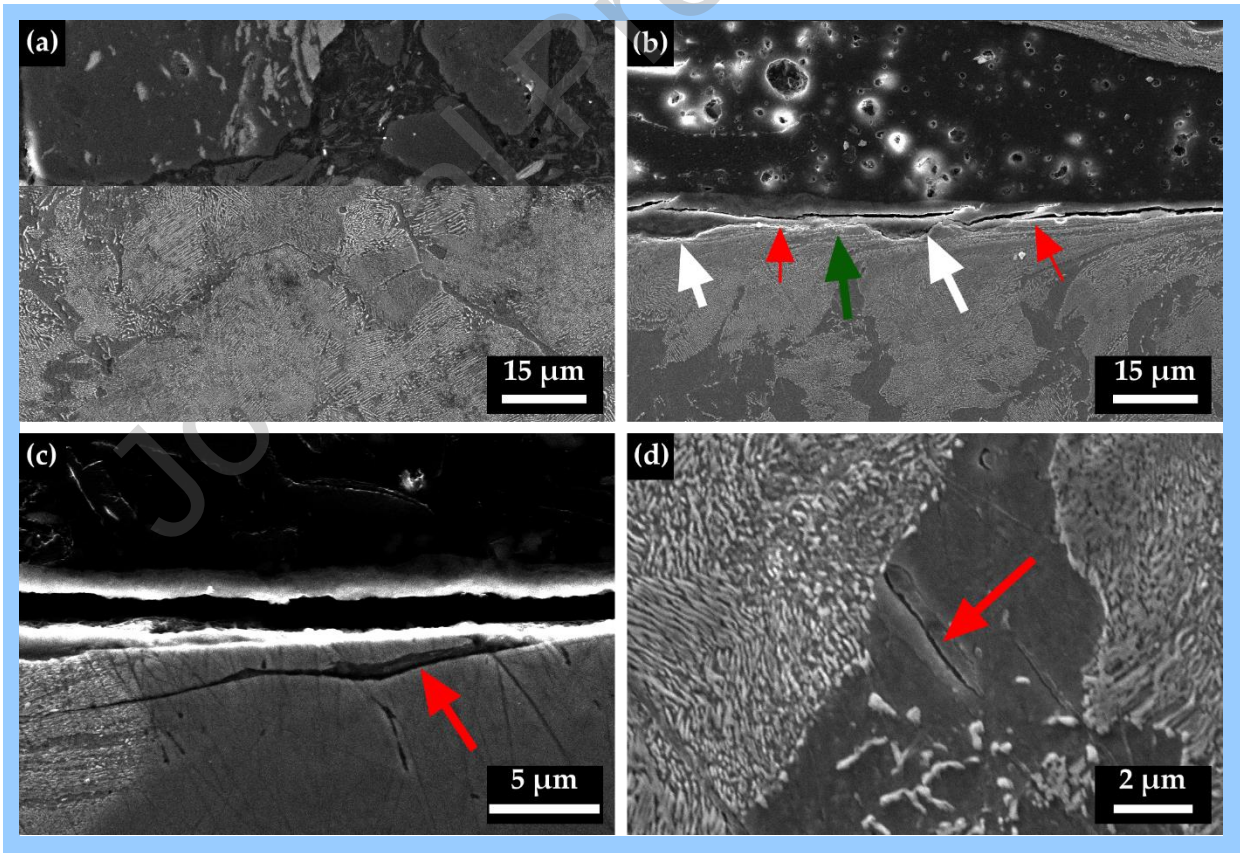

Figure 14 FEG-SEM micrographs of the microstructure observed on the cross-section of the annealed samples before (a) and after wear tests. (b) Overview of the worn sub-surfaces. The white arrows indicate some pits visible on the wear tracks, whereas the red and green

arrows highlight cracks and fragmentation of cementite lamellas, respectively. (c,d) In the order, details of cracks below the worn surfaces and inside the ferritic grain (red arrows).

3.4.5 Microhardness profile

The Vickers microhardness profiles ($HV_{0.05}$) of the cross-sections of all heat-treated samples after wear tests, at different distances (μm) from the sliding interface, are depicted in Figure 15. In all cases, a significant increase in microhardness is observed. For all heat treatment conditions, this increase may be attributed to the occurrence of several phenomena such as strain hardening, a raise in dislocation density, and an increase in shear stresses induced in close proximity of mating surfaces by the sliding motion against the counterbody. For carbide-free bainitic samples, a further increase in microhardness is achieved by the TRIP effect, as demonstrated by XRD measurements of the wear tracks and microstructural analysis of worn cross-sections. The samples austempered at 250 °C exhibits the highest final microhardness. This is due to the highest carbon content in the most stable retained austenite and to the high energy input required to start the bainitic transformation [41]. In addition, in agreement with Hasan et al. [58], the decrease in microhardness in our pearlitic-ferritic microstructure is less sharp than that in the carbide-free bainitic microstructures. The same authors pointed out that, irrespective of the microstructure, the thickness of the hardened layer decreases with decreasing the initial microhardness.

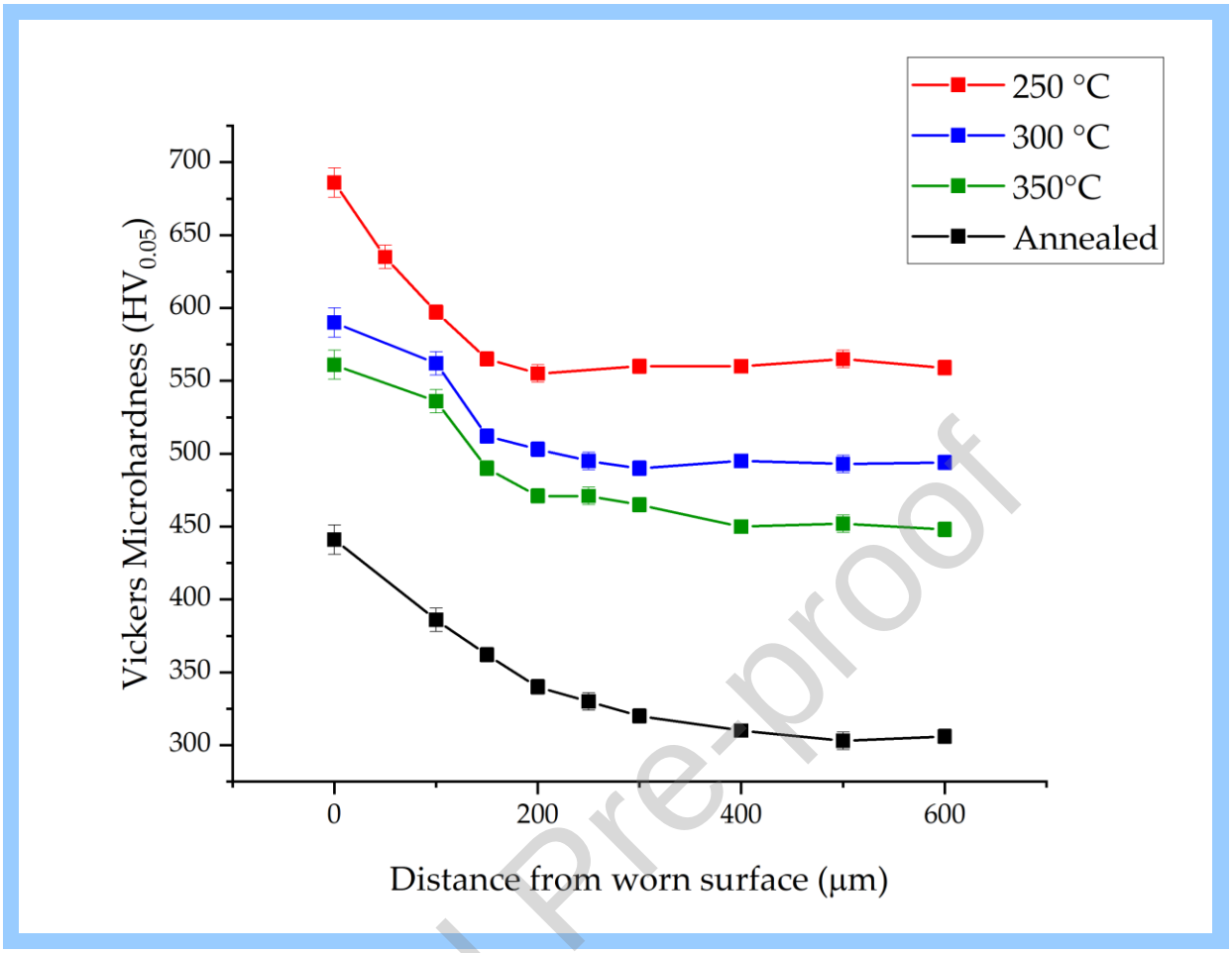

Figure 15 Vickers microhardness profiles ($HV_{0.05}$) of the cross-sections of all heat-treated samples after wear tests, at different distances (µm) from the sliding interface.

4. Conclusions

The wear performance of a high silicon carbide-free bainitic steel with newly developed chemical composition and isothermally treated at temperatures of 200, 250 and 350 °C are investigated and compared with those of a pearlitic-ferritic steel with the same composition. The outputs of the research are as follow:

- Carbide-free bainitic microstructure exhibits lower wear rate in comparison with the pearlitic-ferritic microstructure. The outstanding performance of the carbide-free bainitic microstructure derives from its higher hardness, strain hardening capability and from the TRIP effect. Especially, the strain induced transformation of the C-rich retained austenite into martensite leads to an improve of the tribological properties, through the further hardness increase and the suppression of nucleation.
- By reducing the austempering temperature, the wear rate of the material is also improved thanks to the high microstructural refinement deriving from

the formation of bainite at temperature close to Ms and to the higher mechanical stability of retained austenite.

- Finally, adhesion and tribo-oxidational wear are the main wear mechanisms. The extent of oxidation increases with increasing the austempering temperature and reaches the maximum level for the samples austempered at 350 °C and pearlitic-ferritic microstructure.

Funding: Project supported by the BIRD 2021 program of the University of Padova

References

[1] Mandal D, Ghosh M, Pal J, De PK, Ghosh Chowdhury S, Das SK, et al. Effect of austempering treatment on microstructure and mechanical properties of high-Si steel. J Mater Sci 2009;44:1069–75. https://doi.org/10.1007/s10853-008-3203-z.

[2] Putatunda SK, Singar A V., Tackett R, Lawes G. Development of a high strength high toughness ausferritic steel. Mater Sci Eng A 2009;513–514:329–39. https://doi.org/10.1016/j.msea.2009.02.013.

[3] Caballero FG, Bhadeshia HKDH, Mawella KJA, Jones DG, Brown P. Very strong low temperature bainite. Mater Sci Technol 2002;18:279–84. https://doi.org/10.1179/026708301225000725.

[4] Kapito A, Mostert RJ, Stumpf WE, Siyasiya CW. Carbide-free bainitic steels for rail wheel applications. IOP Conf Ser Mater Sci Eng 2019;655. https://doi.org/10.1088/1757-899X/655/1/012012.

[5] Morales-Rivas L, Garcia-Mateo C, Sourmail T, Kuntz M, Rementeria R, Caballero FG. Ductility of nanostructured bainite. Metals (Basel) 2016;6. https://doi.org/10.3390/met6120302.

[6] Avishan B, Yazdani S, Caballero FG, Wang TS, Garcia-Mateo C. Characterisation of microstructure and mechanical properties in two different nanostructured bainitic steels. Mater Sci Technol (United Kingdom) 2015;31:1508–20. https://doi.org/10.1179/1743284714Y.0000000745.

[7] Leiro A, Vuorinen E, Sundin KG, Prakash B, Sourmail T, Smanio V, et al. Wear of nano-structured carbide-free bainitic steels under dry rolling-sliding conditions. Wear 2013;298–299:42–7. https://doi.org/10.1016/j.wear.2012.11.064.

[8] Efremenko VG, Hesse O, Friedrich T, Kunert M, Brykov MN, Shimizu K, et al. Two-body abrasion resistance of high-carbon high-silicon steel: Metastable austenite vs nanostructured bainite. Wear 2019;418–419:24–35. https://doi.org/10.1016/j.wear.2018.11.003.

[9] Fonstein N. Advanced high strength sheet steels: Physical metallurgy, design, processing, and properties. Switzerlan. Springer, Cham; 2015. https://doi.org/10.1007/978-3-319-19165-2.

[10] Franceschi M, Pezzato L, Gennari C, Fabrizi A, Polyakova M, Konstantinov D, et al. Effect of intercritical annealing and austempering on the microstructure and mechanical properties of a high silicon manganese steel. Metals (Basel) 2020;10:1–19. https://doi.org/10.3390/met10111448.

[11] Edmonds D V., Cochrane RC. Structure-property relationships in bainitic steels. Metall Trans A 1990;21:1527–40. https://doi.org/10.1007/BF02672567.

[12] Son JY, Kim JH, Kim WB, Ye BJ. Effects of austempering conditions on the microstructures and mechanical properties in Fe-0.9%C-2.3%Si-0.3%Mn steel. Met Mater Int 2010;16:357–61. https://doi.org/10.1007/s12540-010-0603-9.

[13] Hase K, Garcia-Mateo C, Bhadeshia HKDH. Bimodal size-distribution of bainite plates. Mater Sci Eng A 2006;438–440:145–8. https://doi.org/10.1016/j.msea.2005.12.070.

[14] Xiong XC, Chen B, Huang MX, Wang JF, Wang L. The effect of morphology on the stability of retained austenite in a quenched and partitioned steel. Scr Mater 2013;68:321–4. https://doi.org/10.1016/j.scriptamat.2012.11.003.

[15] Timokhina IB, Hodgson PD, Pereloma E V. Effect of microstructure on the stability of retained austenite in {TRIP} steels. Metall Mater Trans A 2004;35:2331–40.

[16] Pereloma E V., Gazder AA, Timokhina IB. Addressing retained austenite stability in advanced high strength steels. Mater. Sci. Forum, vol. 738–739, Saint-PeterSburg, Russia: 2013, p. 212–6. https://doi.org/10.4028/www.scientific.net/MSF.738-739.212.

[17] Blondé R, Jimenez-Melero E, Zhao L, Wright JP, Brück E, Van Der Zwaag S, et al. High-energy X-ray diffraction study on the temperature-dependent mechanical stability of retained austenite in low-alloyed TRIP steels. Acta Mater 2012;60:565–77. https://doi.org/10.1016/j.actamat.2011.10.019.

[18] Zhao J, Lv B, Zhang F, Yang Z, Qian L, Chen C, et al. Effects of austempering temperature on bainitic microstructure and mechanical properties of a high-C high-Si steel. Mater Sci Eng A 2019;742:179–89. https://doi.org/10.1016/j.msea.2018.11.004.

[19] Ruiz-jimenez V, Kuntz M, Sourmail T, Caballero FG, Jimenez JA, Garcia-mateo C. Retained Austenite Destabilization during Tempering of Low-Temperature

Bainite 2020.

[20] Santajuana MA, Rementeria R, Kuntz M, Jimenez JA, Caballero FG, Garcia-Mateo C. Low-Temperature Bainite: A Thermal Stability Study. Metall Mater Trans A Phys Metall Mater Sci 2018;49:2026–36. https://doi.org/10.1007/s11661-018-4595-2.

[21] Santofimia MJ, Zhao L, Sietsma J. Microstructural evolution of a low-carbon steel during application of quenching and partitioning heat treatments after partial austenitization. Metall Mater Trans A Phys Metall Mater Sci 2009;40:46–57. https://doi.org/10.1007/s11661-008-9701-4.

[22] Edmonds D V. Advanced bainitic and martensitic steels with carbide-free microstructures containing retained austenite. Mater Sci Forum 2010;638–642:110–7. https://doi.org/10.4028/www.scientific.net/MSF.638-642.110.

[23] Ławrynowicz Z. Carbon partitioning during bainite transformation in low alloy steels. Mater Sci Technol 2002;18:1322–4. https://doi.org/10.1179/026708302225007259.

[24] Guo H, Zhao A, Zhi C, Ding R, Wang J. Two-body abrasion wear mechanism of super bainitic steel. Mater Sci Technol (United Kingdom) 2017;33:893–8. https://doi.org/10.1080/02670836.2016.1245239.

[25] Sourmail T, Caballero FG, Garcia-Mateo C, Smanio V, Ziegler C, Kuntz M, et al. Evaluation of potential of high Si high C steel nanostructured bainite for wear and fatigue applications. Mater Sci Technol (United Kingdom) 2013;29:1166–73. https://doi.org/10.1179/1743284713Y.0000000242.

[26] Chang LC. The rolling/sliding wear performance of high silicon carbide-free bainitic steels. Wear 2005;258:730–43. https://doi.org/10.1016/j.wear.2004.09.064.

[27] Wang TS, Yang J, Shang CJ, Li XY, Lv B, Zhang M, et al. Sliding friction surface microstructure and wear resistance of 9SiCr steel with low-temperature austempering treatment. Surf Coatings Technol 2008;202:4036–40. https://doi.org/10.1016/j.surfcoat.2008.02.013.

[28] Yang J, Wang TS, Zhang B, Zhang FC. Sliding wear resistance and worn surface microstructure of nanostructured bainitic steel. Wear 2012;282–283:81–4. https://doi.org/10.1016/j.wear.2012.02.008.

[29] Moghaddam PV, Rinaudo M, Hardell J, Vuorinen E, Prakash B. Influence of fracture toughness on two-body abrasive wear of nanostructured carbide-free bainitic steels. Wear 2020;460–461:203484.

https://doi.org/10.1016/j.wear.2020.203484.

[30] Jin N, Clayton P. Effect of microstructure on rolling/sliding wear of low carbon bainitic steels. Wear 1997;202:202–7. https://doi.org/10.1016/S0043-1648(96)07271-7.

[31] Toloui M, Militzer M. Phase field modeling of the simultaneous formation of bainite and ferrite in TRIP steel. Acta Mater 2018;144:786–800. https://doi.org/10.1016/j.actamat.2017.11.047.

[32] Qian L, Zhou Q, Zhang F, Meng J, Zhang M, Tian Y. Microstructure and mechanical properties of a low carbon carbide-free bainitic steel co-alloyed with Al and Si. Mater Des 2012;39:264–8. https://doi.org/10.1016/j.matdes.2012.02.053.

[33] Franceschi M, Pezzato L, Gennari C, Brunelli K, Dabal M. STUDIO DELL'EVOLUZIONE MICROSTRUTTURALE E DELLE CARATTERISTICHE MECCANICHE DI ACCIAI AD ALTO SILICIO AUSTEMPERATI. 38mo Convegno Naz. AIM, 2021.

[34] Franceschi M, Miotti Bettanini A, Pezzato L, Dabalà M, Jacques PJ. Effect of Multi-Step Austempering Treatment on the Microstructure and Mechanical Properties of a High Silicon. Metals (Basel) 2021;11:17. https://doi.org/https://doi.org/ 10.3390/met11122055.

[35] Lutterotti L. Maud: a Rietveld analysis program designed for the internet and experiment integration. Acta Crystallogr Sect A Found Crystallogr 2000;56:s54–s54. https://doi.org/10.1107/s0108767300021954.

[36] Dyson D.J., Holmes B. Effect of alloying additions on the lattice parameter of austenite. J Iron Steel Inst 1970;208:469–74.

[37] Eres-Castellanos A, Morales-Rivas L, Jimenez JA, Caballero FG, Garcia-Mateo C. Effect of Ausforming on the Macro- and Micro-texture of Bainitic Microstructures. Metall Mater Trans A Phys Metall Mater Sci 2021;52:4033–52. https://doi.org/10.1007/s11661-021-06363-w.

[38] Conshohocken W. Standard Test Method for Wear Testing with a Pin-on-Disk Apparatus 1. Wear 2007;05:1–5. https://doi.org/10.1520/G0099-17.Copyright.

[39] Skowronek A, Morawiec M, Ruiz-Jimenez V, Garcia-Mateo C, Grajcar A. Physical simulation and dilatometric study of double-step heat treatment of medium-Mn steel. Arch Civ Mech Eng 2020;20:1–11. https://doi.org/10.1007/s43452-020-00144-9.

[40] Garcıa-Mateo C, Caballero FG. Ultra-high–strength Bainitic Steels 2005;45:1736–40.

[41] Bhadeshia HKDH. Bainite in steels: theory and practice. vol. 19. Maney Publishing; 2006.

[42] Materials T, Company I. ASM Handbook Volume 04: Heat Treating n.d.

[43] He SH, He BB, Zhu KY, Huang MX. On the correlation among dislocation density, lath thickness and yield stress of bainite. Acta Mater 2017;135:382–9. https://doi.org/10.1016/j.actamat.2017.06.050.

[44] Valizadeh Moghaddam P, Hardell J, Vuorinen E, Prakash B. Dry sliding wear of nanostructured carbide-free bainitic steels – Effect of oxidation-dominated wear. Wear 2020;454–455:203317. https://doi.org/10.1016/j.wear.2020.203317.

[45] Caballero FG, Garcıa-Mateo C. The Role of Retained Austenite on Tensile Properties of Steels with Bainitic Microstructures. Mater Trans 2005;46:1839–46.

[46] Putatunda SK. Influence of austempering temperature on microstructure and fracture toughness of a high-carbon, high-silicon and high-manganese cast steel. Mater Des 2003;24:435–43. https://doi.org/10.1016/S0261-3069(03)00090-6.

[47] Grajcar A, Krztoń H. Effect of isothermal bainitic transformation temperature on retained austenite fraction in C-Mn-Si-Al-Nb-Ti TRIP-type steel Manufacturing and processing. 2009.

[48] Long X, Zhao G, Zhang F, Xu S, Yang Z, Du G, et al. Evolution of tensile properties with transformation temperature in medium-carbon carbide-free bainitic steel. Mater Sci Eng A 2020;775:138964. https://doi.org/10.1016/j.msea.2020.138964.

[49] Quinn TFJ. Oxidational wear modelling: Part II. The general theory of oxidational wear. Wear 1994;175:199–208. https://doi.org/10.1016/0043-1648(94)90183-X.

[50] Adams MJ. Introduction to Tribology 36/3. Tribol Int 2003;36:559. https://doi.org/10.1016/s0301-679x(02)00183-4.

[51] Moghaddam PV, Hardell J, Vuorinen E, Prakash B. Effect of retained austenite on adhesion-dominated wear of nanostructured carbide-free bainitic steel. Tribol Int 2020;150:106348. https://doi.org/10.1016/j.triboint.2020.106348.

[52] Das Bakshi S, Leiro A, Prakash B, Bhadeshia HKDH. Dry rolling/sliding wear of nanostructured bainite. Wear 2014;316:70–8.

https://doi.org/10.1016/j.wear.2014.04.020.

[53] Moghaddam PV, Hardell J, Vuorinen E, Prakash B. The role of retained austenite in dry rolling/sliding wear of nanostructured carbide-free bainitic steels. Wear 2019;428–429:193–204. https://doi.org/10.1016/j.wear.2019.03.012.

[54] Leiro A, Kankanala A, Vuorinen E, Prakash B. Tribological behaviour of carbide-free bainitic steel under dry rolling/sliding conditions. Wear 2011;273:2–8. https://doi.org/10.1016/j.wear.2011.03.025.

[55] Zhao J, Zhang F, Lv B, Yang Z, Chen C, Long X, et al. Inconsistent effects of austempering time within transformation stasis on monotonic and cyclic deformation behaviors of an ultrahigh silicon carbide-free nanobainite steel. Mater Sci Eng A 2019;751:80–9. https://doi.org/10.1016/j.msea.2019.01.100.

[56] Neog SP, Bakshi S Das, Das S. Effect of normal loading on microstructural evolution and sliding wear behaviour of novel continuously cooled carbide free bainitic steel. Tribol Int 2021;157:106846. https://doi.org/10.1016/j.triboint.2020.106846.

[57] Das Bakshi S, Shipway PH, Bhadeshia HKDH. Three-body abrasive wear of fine pearlite, nanostructured bainite and martensite. Wear 2013;308:46–53. https://doi.org/10.1016/j.wear.2013.09.008.

[58] Hasan SM, Chakrabarti D, Singh SB. Dry rolling/sliding wear behaviour of pearlitic rail and newly developed carbide-free bainitic rail steels. Wear 2018;408–409:151–9. https://doi.org/10.1016/j.wear.2018.05.006.

CRediT authorship contribution statement

Mattia Franceschi: Methodology, Formal analysis, Software**,** Data curation, Writing- Original draft preparation, Writing - Review & Editing. **Luca Pezzato**: Visualization, Investigation, Writing - Review & Editing. ***Annalisa Fortini****:* Investigation, Writing - Review & Editing, Formal Analysis, Methodology. **Chiara Soffritti**: Software, Formal Analysis, Data curation, Writing- Original draft preparation, Writing - Review & Editing. **Gian Luca Garagnani**: project administration, supervision. **Manuele Dabalà**: methodology, data curation, project administration, funding acquisition.

Declaration of interests

☒ The authors declare that they have no known competing financial interests or personal relationships that could have appeared to influence the work reported in this paper.

☐The authors declare the following financial interests/personal relationships which may be considered as potential competing interests:

originality

The paper has not been published previously, that it is not under consideration for publication elsewhere, and that if accepted it will not be published elsewhere in the same form, in English or in any other language, without the written consent of the publisher.

2) The paper does not contain material which has been published previously, by the current authors or by others, of which the source is not explicitly cited in the paper.

Highlights

- Wear resistance of newly designed carbide-free bainitic (CFB) steels
- Effect of heat treatment, morphology and content of microstructural constituents
- Carbide-free bainitic steels exhibited the lowest wear rates
- Superior performance of CFB steels due to transformation induced plasticity effect
- Adhesion and tribo-oxidational as the main wear mechanisms